Journal of Naval Architecture and Marine Engineering
December, 2021
http://dx.doi.org/10.3329/jname.v18i2.51972 *http://www.banglajol.info*

A COMPUTATIONAL STUDY ON FLOW CHARACTERISTICS AND ENERGY DISTRIBUTION IN A ROTATING COILED RECTANGULAR DUCT WITH LONGITUDINAL VORTEX GENERATION

R. K. Chanda[1], M. S. Hasan[2], M. M. Alam[3], R. N. Mondal[1]

[1]Department of Mathematics, Jagannath University, Dhaka-1100, Bangladesh, Email: ratan222003@gmail.com, rnmondal71@yahoo.com

[2]Department of Mathematics, Bangabandhu Sheikh Mujibur Rahman Science and Technology University, Gopalganj-8100, Bangladesh, Email: sanjeedlhasan@gmail.com

[3]Mathematics Discipline, Khulna University, Khulna-9208, Bangladesh, Email: alam_mahmud2000@yahoo.com

Abstract:

Investigation on fluid flow and energy distribution in a rotating coiled rectangular duct (CRD) with differentially heated horizontal walls has been analyzed numerically by using a spectral-based numerical scheme. The system is rotated around the vertical axis in the clockwise direction over the Taylor number (Tr) ranging from 0 to 2000 keeping the other parameters constant as aspect ratio Ar =3, curvature ratio β = 0.5, the Dean number Dn = 1000 and the Prandtl number Pr = 7.0 (water). To reveal steady solution (SS) curves, we applied path continuation technique and obtained five asymmetric SS curves comprising with 2- to 8-pair cell. A bar diagram is also drawn to visualize, at a glance, longitudinal vortex generation on various curves of steady solutions. To explore unsteady behavior, time-progression analysis is performed and flow characteristics are precisely determined by obtaining phase space trajectory of the solutions. The transient flow demonstrates various stages of physically realizable solutions including chaotic, multi-periodic, periodic and steady-state; and it is found that the number of secondary vortices declines as Tr is increased. Convective heat transfer (CHT) is computed and the corresponding dependence on the flow stages is discussed accurately. Finally, a comparison has been made between the numerical computation and experimental investigations which shows a benchmark agreement.

Keywords: Rotating curved duct, Taylor number, velocity contour, energy distribution, chaotic.

1. Introduction

Fluid involving various flow characteristics and HT through CDs at rotating stage have an unbounded usage in fluids engineering, namely in chemical, mechanical, biomechanical, and biological engineering e.g., rotating-machinery, nuclear engineering, heat exchangers, gas turbines, electric generators, etc. Centrifugal forces due to channel curvature attribute twisted flow known as secondary flow (SF). Because of Coriolis and centrifugal forces, two types of secondary forces are produced and the influence of these two forces generates intricately shaped of the SF and the axial flow (AF) is observed. The SF is characterized by Dean vortices that were first originated by Dean (1927, 1928). After that several researchers have studied these flows using various experimental (Ligrani and Niver, 1988, Yamamoto et al., 2006 and Sugiyama et al., 1983) numerical and experimental (Bara et al., 1992, Wang and Yang, 2004, 2005 and Li et al., 2016), analytical and experimental (Baylis, 1971 and Humphrey et al., 1977) and numerical (Berger et al., 1983, Nandakumar and Masliyah, 1986, Ito, 1987, Yanase et al., 2002 and Mondal, 2007) techniques.

In order to study the branching structure of SS, an extensive work of Mondal et al. (2007) presented the branching pattern of the flow in a CD of square cross-section more precisely. In this regard, Ludwieg (1951) analyzed the flow in a co-rotating square CD by integrating the monument equations. Daskopoulos and Lenhoff (1989), Mondal (2006) studied detailed the bifurcation diagram through CRD. Miyazaki (1971, 1973) has presented a numerical study of the characteristics fluid flow in rotating CD with positive rotation for investigating HT of the flow in both circular and rectangular cross-section. A remarkable number of articles have been published on CSD (Cheng et al., 1975 and Shantini and Nandakumar, 1986) and on CRD (Yanase et al., 2002). Related to rotation and curvature of the duct for two-dimensional flow in a confined geometry, e.g. a square and rectangular-shaped duct, several researchers have been conducted. Selmi et al. (1994, 1999) revealed

1813-8535 (Print), 2070-8998 (Online) Received on: February 2021

the latest studies on the flows in a rotating CRD. Yanase et al. (2002) conducted a magnificent study for combined solution structure of fluid flow through a CRD of large *Ar*. A detailed pore-scale study using spectral-based method on combined flow branching shape with linear stability is available in literature by Mondal et al. (2006). They established a potential connection between the time-dependent solution and the combined solution structure consisting of steady solution branches. Hasan et al. (2021) addressed this issue by developing flow formations for non-isothermal flows. To obtain reliable and meaningful characteristics and to get a better fundamental understanding of swirling flow, an advanced numerical simulations model based on 3D vortex structures is used by Chandratilleke et al. (2012). Watanabe and Yanase (2013) described bifurcation phenomena for a square geometry for both two- and three-dimensional analysis.

In order to understand the behavior of transient flow, some remarkable analysis has been carried out for various physical domains. Yanase and Nishiyama (1988) performed oscillating behavior of CD flows for rectangular cross-section. Related to oscillating behavior in a confined geometry, e.g., rectangular duct or channel, several works have been conducted. Yanase et al. (2005, 2008) and recently Mondal et al. (2017) investigated oscillation properties numerically. Wang and Yang (2004, 2005) reported an extensive study with numerical analysis for determining oscillation behaviors of the flow through a CSD using a flow visualization technique. Mondal et al. (2015, 2021) conducted a numerical prognosis of the oscillation behavior by time advancement for considering square and rectangular configurations and discussed detailed transitions between periodic and aperiodic oscillating and instability of the oscillating behavior. Recently, Nowruzi et al. (2019) applied the Homotopy perturbation method to investigate hydrodynamic instability in CRD of small Ar for several curvatures. Their study was unable to focus on the influence of the parameters in flow transition and velocity. However, the effects of rotation in fluid flow as well as branching structure and oscillating behavior of flow are still absent in literature for a rotating CRD flow of moderate Ar; which attracted the authors to fill in the gap.

The mentionable applications of flows in various CDs are to promote HT in the fluid causing Dean vortices. Chandratilleke and Nursubyakto (2003) conducted a numerical analysis to explain properties of swirling flow in a CD of Ars (1 - 8) where heated outer wall. Considering the effects of SF, Ray et al. (2020) performed flow oscillating behavior through CRD and recognized that SFs enhance HT. Mondal et al. (2007) studied the oscillating behavior of the thermal flow in a CSD numerically. The authors investigated the SF structure and the effects of HT performance. A numerical procedure, known as FDM, is used by Zhang et al. (2018) to investigate the time-dependent CHT and mixing between two different geometries. The present study covers SS structure as well as transient solutions with CHT in CRD at the rotating stage with the effects of centrifugal and Coriolis instability on flow transition.
In the ongoing exploration, the progression of the complex flow behaviors in the critical points of the SS curves as well as the thermal flow transition in a CRD with strong curvature while identifying the influence from the various flow and geometrical parameters is investigated for different Taylor numbers. The main purpose of this study is to pursuit solution formation of SS and explores transient behavior with heat-flux properties of secondary vortices (SV) on CHT. The study articulates and verifies an advanced approach for a computational scheme to identify hydrodynamic variability in a CRD reflected by the generation of Dean vortices.

2. Governing Equations and Flow Model

The system under consideration is presented schematically. Figure 1 illustrates the cross-sectional view and the coordinate system; here *h* and *d* denote the half height and width respectively with necessary notations Ω_T ; the angular velocity. The fluid passes through uniformly in the steam-wise direction. The set of governing equations for the flow and HT are

Continuity equation:

$$\frac{\partial u'}{\partial r'}+\frac{\partial v'}{\partial y'}+\frac{u'}{r'}=0 \tag{1}$$

Momentum equations:

$$\frac{\partial u'}{\partial t'}+u'\frac{\partial u'}{\partial r'}+v'\frac{\partial u'}{\partial y'}-\frac{w'^2}{r'}-2\Omega_T w'=-\frac{1}{\rho}\frac{\partial P'}{\partial r'}+\upsilon\left[\frac{\partial^2 u'}{\partial r'^2}+\frac{\partial^2 u'}{\partial y'^2}+\frac{1}{r'}\frac{\partial u'}{\partial r'}-\frac{u'}{r'^2}\right] \tag{2}$$

$$\frac{\partial v'}{\partial t'}+u'\frac{\partial v'}{\partial r'}+v'\frac{\partial v'}{\partial y'}=-\frac{1}{\rho}\frac{\partial P'}{\partial y'}+\upsilon\left[\frac{\partial^2 v'}{\partial r'^2}+\frac{1}{r'}\frac{\partial v'}{\partial r'}+\frac{\partial^2 v'}{\partial y'^2}\right]+g\delta T' \tag{3}$$

$$\frac{\partial w'}{\partial t'}+u'\frac{\partial w'}{\partial r'}+v'\frac{\partial w'}{\partial y'}+\frac{u'w'}{r'}+2\Omega_T u'=-\frac{1}{\rho}\frac{1}{r'}\frac{\partial P'}{\partial z'}+\upsilon\left[\frac{\partial^2 w'}{\partial r'^2}+\frac{\partial^2 w'}{\partial y'^2}+\frac{1}{r'}\frac{\partial w'}{\partial r'}-\frac{w'}{r'^2}\right] \tag{4}$$

Energy equation:

$$\frac{\partial T'}{\partial t'}+u'\frac{\partial T'}{\partial r'}+v'\frac{\partial T'}{\partial y'}=\kappa\left[\frac{\partial^2 T'}{\partial r'^2}+\frac{1}{r'}\frac{\partial T'}{\partial r'}+\frac{\partial^2 T'}{\partial y'^2}\right] \tag{5}$$

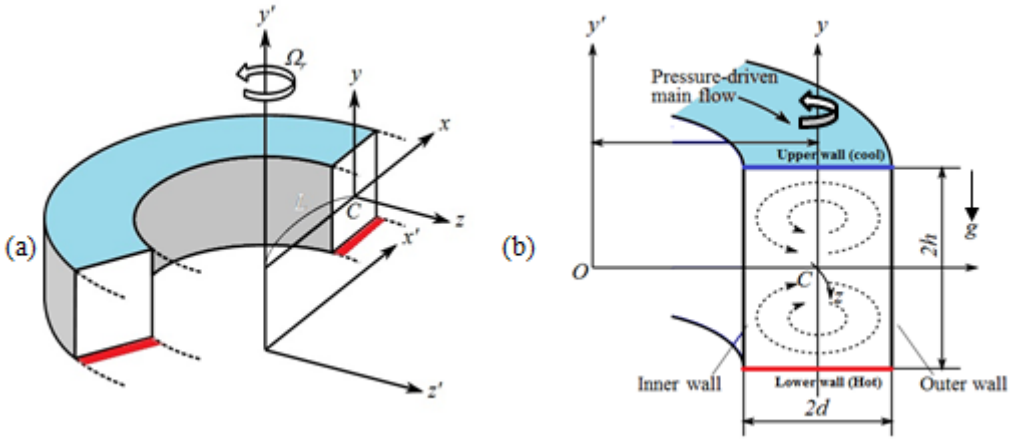

Fig. 1: (a) Coordinate system, (b) Cross-sectional view

where, $r'=L+lx'$ and the prime $(')$ denotes the dimensional variables. The dimensional variables are then non-dimensionalized by using the representative length d, the representative velocity $U_0=\frac{\upsilon}{d}$, where υ is the kinematic viscosity of the fluid. We introduce the non-dimensional variables defined as

$$u=\frac{u'}{U_0},v=\frac{v'}{U_0},\eta=\frac{\sqrt{2\beta}}{U_o}\eta',\ x=\left(\frac{x'}{d}-\frac{1}{\beta}\right),y=\frac{y'}{d},z=\frac{z'}{d},\ \theta=\frac{\theta'}{\Delta\theta'},\ t=\frac{U_0}{d}t',\ \beta=\frac{d}{L},\ P=\frac{P'}{\rho\ U_0^{\ 2}}$$

where u,v and η are the non-dimensional velocity components in the x,y and z directions, respectively; The stream function which satisfies equation (1) is:

$$u=\frac{1}{1+\beta x}\frac{\partial\psi}{\partial y},\ v=-\frac{1}{1+\beta x}\frac{\partial\psi}{\partial x}\Bigg\} \tag{6}$$

Then, the derived equations for axial velocity (η), stream function (ψ) and temperature (θ) as:

$$(1+\beta x)\frac{\partial\eta}{\partial t}=Dn-\frac{1}{3}\frac{\partial(\eta,\psi)}{\partial(x,y)}-\frac{\beta^2\eta}{1+\beta x}+(1+\beta x)\Delta_2\eta-\frac{\eta}{3(1+\eta x)}\frac{\partial\psi}{\partial y}\eta+\beta\frac{\partial\eta}{\partial x}-\beta Tr\frac{\partial\psi}{\partial y} \tag{7}$$

$$\left(\Delta_2-\frac{\beta}{1+\beta x}\frac{\partial}{\partial x}\right)\frac{\partial\psi}{\partial t}=-\frac{1}{3(1+\beta x)}\frac{\partial(\Delta_2\psi,\psi)}{\partial(x,y)}+\frac{\beta}{3(1+\beta x)^2}\left[\frac{\partial\psi}{\partial y}\left(2\Delta_2\psi-\frac{3\beta}{1+\beta x}\frac{\partial\psi}{\partial x}+\frac{\partial^2\psi}{\partial x^2}\right)-\frac{\partial\psi}{\partial x}\frac{\partial^2\psi}{\partial x\partial y}\right]+\frac{\beta}{(1+\beta x)^2}\left[3\beta\frac{\partial^2\psi}{\partial x^2}-\frac{3\beta^2}{1+\beta x}\frac{\partial\psi}{\partial x}\right] \tag{8}$$

$$-\frac{2\beta}{1+\beta x}\frac{\partial}{\partial x}\Delta_2\psi+\frac{1}{3}\eta\frac{\partial\eta}{\partial y}+\Delta_2{}^2\psi-Gr\ (1+\beta x)\frac{\partial\theta}{\partial x}+\frac{1}{3}Tr\frac{\partial\eta}{\partial y},$$

$$\frac{\partial\theta}{\partial t}=\frac{1}{\mathrm{Pr}}\left(\Delta_2\theta+\frac{\beta}{1+\beta x}\frac{\partial\theta}{\partial x}\right)-\frac{1}{3(1+\beta x)}\frac{\partial(\theta,\psi)}{\partial(x,y)} \tag{9}$$

where, $\Delta_2 \equiv \frac{\partial^2}{\partial x^2} + \frac{1}{9}\frac{\partial^2}{\partial y^2}, \qquad \frac{\partial(f,g)}{\partial(x,y)} \equiv \frac{\partial f}{\partial x}\frac{\partial g}{\partial y} - \frac{\partial f}{\partial y}\frac{\partial g}{\partial x}.$ (10)

In equations (7) to (9), the dimensionless parameters, *Dn*, *Tr*, *Gr* and Pr are defined as

$$Dn = \frac{Gd^3}{\mu\upsilon}\sqrt{\frac{2d}{L}}\ ,\ Gr = \frac{\xi g \Delta\theta d^3}{\upsilon^2},\ Tr = \frac{2\sqrt{2\beta}\Omega_T d^3}{\upsilon\beta},\ \Pr = \frac{\upsilon}{\kappa} \tag{11}$$

The dimensionless boundary conditions for η, ψ and θ are

$$\eta = \psi = \frac{\partial\psi}{\partial x} = 0 \quad \text{at} \quad x = \pm 1, y = y \tag{12a}$$

$$\eta = \psi = \frac{\partial\psi}{\partial y} = 0 \quad \text{at} \quad x = x, y = \pm 1 \tag{12b}$$

$$\theta = 1 \quad \text{at} \quad x = x, y = 1 \tag{12c}$$

$$\theta = -1 \quad \text{at} \quad x = x, y = -1 \tag{12d}$$

$$\theta = -y \quad \text{at} \quad x = \pm 1, y = y \tag{12e}$$

3. Numerical Analysis

3.1 Method of numerical design

To derive numerical solution from the equations (7) - (9), spectral approach is applied [29]. According to the fundamental concept of spectral and collocation approach, the series functions containing the Chebyshev polynomials are used in the *x* and *y* directions where *x* and *y* are variables. That is, the expansion functions $\phi_n(x)$ and $\psi_n(x)$ are stated as

$$\left.\begin{aligned}\phi_n(x) &= (1-x^2)F_n(x),\\ \psi_n(x) &= (1-x^2)^2 F_n(x)\end{aligned}\right\} \tag{13}$$

where, $F_n(x) = \cos\left(n\cos^{-1}(x)\right)$ is the n[th] order Chebyshev polynomial, $\eta(x,y,t)$, $\psi(x,y,t)$ and $\theta(x,y,t)$ are expanded as

$$\left.\begin{aligned}\eta(x,y,t) &= \sum_{m=0}^{M}\sum_{n=0}^{N}\eta_{mn}(t)\phi_m(x)\phi_n(y)\\ \psi(x,y,t) &= \sum_{m=0}^{M}\sum_{n=0}^{N}\psi_{mn}(t)\psi_m(x)\psi_n(y).\\ \theta(x,y,t) &= \sum_{m=0}^{M}\sum_{n=0}^{N}\theta_{mn}(t)\phi_m(x)\phi_n(y) - y\end{aligned}\right\} \tag{14}$$

To achieve steady solution $\eta(x,y)$, $\psi(x,y)$ and $\theta(x,y)$ the expansion series (14) with coefficients η_{mn}, ψ_{mn} and θ_{mn} are transformed into the basic equations (7) - (9) abide by applying the collocation method. Finally, to attain unsteady solutions, the Crank-Nicolson and Adams-Bashforth methods composed with the function expansion (14) and the collocation methods are applied to Eqs. (7) to (9).

3.2 Hydraulic resistance coefficient

The resistant coefficient or *hydraulic resistance coefficient* defined as

$$\frac{p_1^* - p_2^*}{\Delta z^*} = \frac{\lambda}{d_h^*}\frac{1}{2}\rho\left\langle\eta^*\right\rangle^2 \tag{15}$$

where, $\langle\ \rangle$ positions for the mean over the cross-section of the duct and d_h^* is the hydraulic diameter, and $\langle \eta^* \rangle$ is the stream-wise main velocity deliberated by

$$\langle \eta^* \rangle = \frac{\nu}{4\sqrt{2\beta}d} \int_{-1}^{1} dx \int_{-1}^{1} \eta(x,y,t)dy \tag{16}$$

λ is linked to the average of the dimensionless stream-wise velocity $\langle \eta \rangle = \sqrt{2\beta}d \langle \eta^* \rangle / \nu$ as

$$\lambda = \frac{16\sqrt{2\beta}Dn}{3\langle \eta \rangle^2} \tag{17}$$

3.3 Grid sensitivity test

Summary of 5 (five) test cases using truncation numbers *M* and *N*, the comparative study is conducted at 5 truncation numbers. The computational domain size in this study is 14×42, 16×48, 18×54, 20×60 and 22×66 i.e., *N* is chosen equal to 3*M*. The grid resolution, quantified by 20×60, was sufficiently fine to ensure accuracy of the solutions as represented Table 1.

Table 1: λ and $\eta(0,0)$ for various *M* and *N* at $Dn = 1000, Gr = 100$, Tr = 200 and $\beta = 0.5$

M	*N*	λ	$\eta(0,0)$
14	42	0.3431509495	1069.544566
16	48	0.3432371976	1070.025634
18	54	0.3433102861	1070.551156
20	**60**	**0.3433202265**	**1070.720377**
22	66	0.3433191600	1070.749269

4. Results and Discussion

4.1 Combined structure of steady solutions

The combined flow structure of the solution curves is investigated comprehensively for β = 0.5. By carefully examining the data, we have found asymmetric five branches of solution curves for *Dn* = 1000, *Gr* = 100 and 0 ≤ Tr ≤ 2000. The whole process of various values of *Tr* ranging from 0 to 2000 results in a complex bifurcation diagram as presented in Figure 2(a). The five solution curves are named the 1st solution curve, the 2nd solution curve, the 3rd solution curve, the 4th solution curve and the 5th solution curve, respectively. To visualize the perplexing curve structure as well as to categorize the solution curves from each other, Figure 2(b) represents the amplification of Fig. 2(a). Figure 3 displays velocity contours and energy distribution (temperature profile) for various values of *Tr*. In this section, we discuss the five solution curves and their flow patterns in brief.

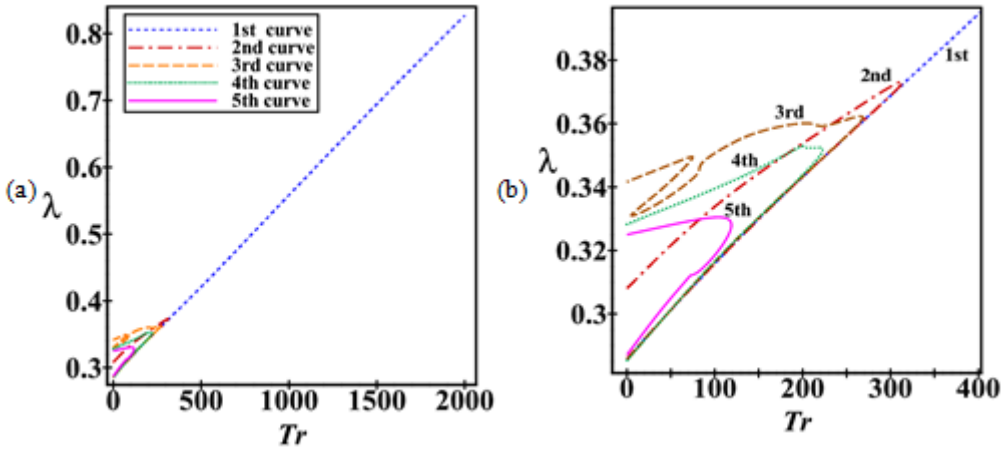

Fig. 2: Schematic of the combined flow structure and amplification for β = 0.5, *Dn* = 1000, *Gr* = 100 and 0 ≤ *Tr* ≤ 2000. (a) Solution structure of SSs, (b) Amplification of Fig. 2a around *Tr* = 200.

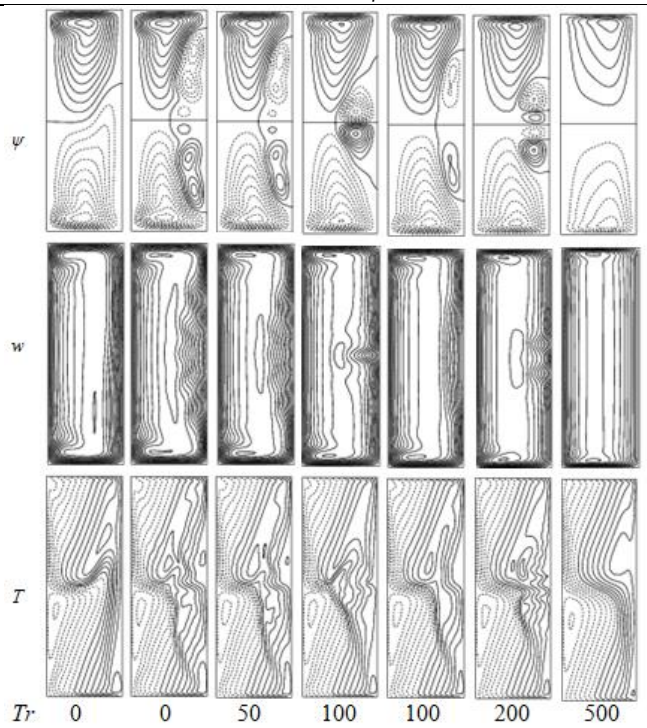

Fig. 3: Contour plots of Streamlines: top, secondary flow; middile, axial flow; bottom, energy distribution on the five solution curves for different values of Tr.

4.1.1 The first solution curve

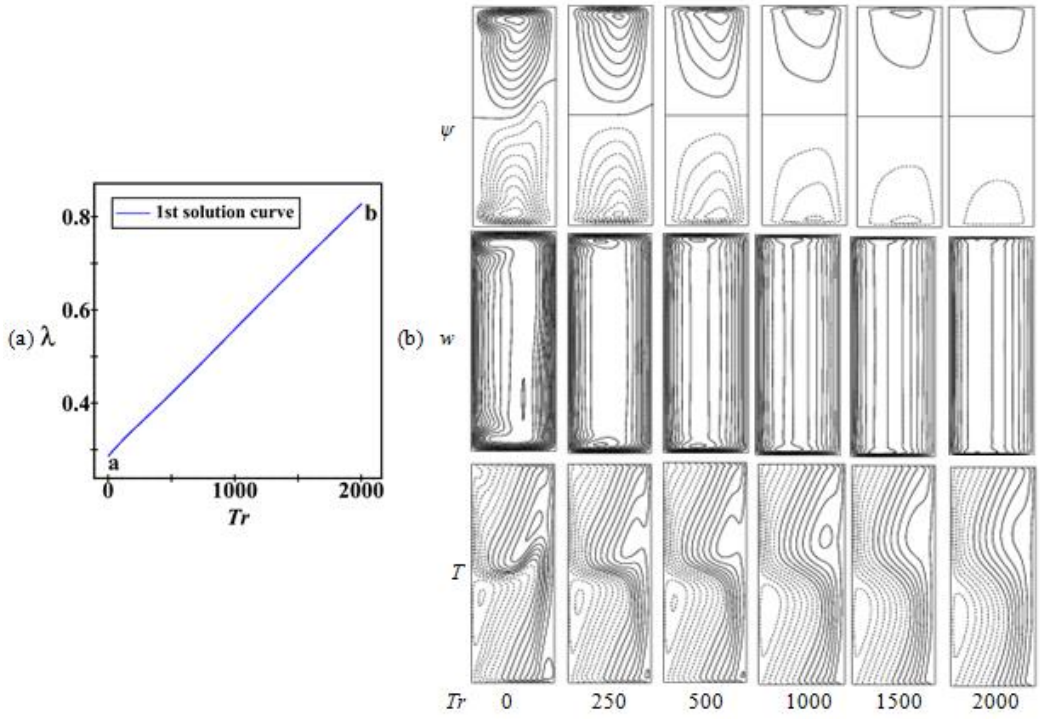

Fig. 4: (a) The 1st solution curve for $\beta = 0.5$ and $0 \leq Tr \leq 2000$ (b) SF (top), AF (middle) and energy distribution (bottom) for different Tr at $\beta = 0.5$.

The 1st solution curve is illustrated by a solid blue-colored line in Figure 4(a) for $\beta = 0.5$ and $0 \leq Tr \leq 2000$. The only branch of this study that occupies the entire range of Tr and there is no turning to its route as presented in Fig. 4(a). After that, in order to observe the configurations and dissimilarities on the 1st solution curve, typical

contours of velocity profiles and energy distribution are presented at different values of *Tr* in Fig. 4(b). It can be seen that the solution curve contains asymmetric and symmetric single-pair cell vortex solution. The velocity contour is strongly asymmetric single-pair cell vortex for smaller values of *Tr* but asymmetry disappears with the increase of *Tr* as a result the flow pattern becomes symmetric. Strong centrifugal force causes asymmetric of SF. On the other hand, the Coriolis force intensifies with the inrease of *Tr* . The interaction to each other of the two forces stabilizes them which causing symmetry in the SF. It should be remarked that, the streamlines (solid and dotted lines) of the SF gradually reduces with the increasing of *Tr* which appeares upper and lower section of the duct.

4.1.2 The second solution curve

The 2nd SS curve for $0 \leq Tr \leq 2000$ is presented by a red-colored solid line in Figure 5(a). Note that, this solution curve exists for a small range of *Tr* which starts from $Tr = 0$ and finally return to a point *c* with a single smooth turning point at point *b* ($Tr \approx 313.920270$); (see Fig. 5(a)). Figure 5(b) shows velocity profiles and energy distribution on the 2nd solution curve at different *Tr*. It is observed that, this curve consists of asymmetric and nearly symmetric 1- and 2-pair cell solution and the solution curve of the upper part (from point *a* to *b*) is different from the lower part (from point *b* to *c*) at the same value of *Tr*. The shape of AF looks like dumbbell.

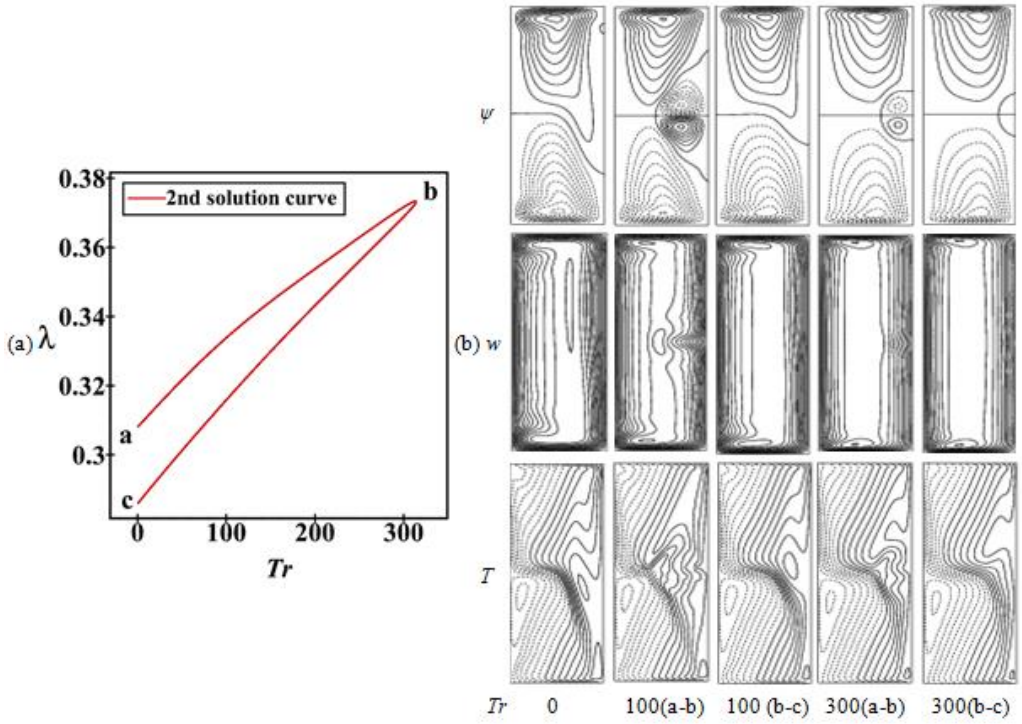

Fig. 5: (a) The 2nd solution curve for $\beta = 0.5$ and $0 \leq Tr \leq 2000$ (b) SF (top), AF (middle) and energy distribution (bottom) for different *Tr* at $\beta = 0.5$.

4.1.3 The third solution curve

The 3rd SS curve is depicted by a golden-colored solid line whose position is for small *Tr*; (see Fig. 6(a)). Clearly, the all turning points turn very gently. As visualized in Fig. 6(b), the third solution curve consists of asymmetric single-pair cell vortex and symmetric 2- to 4-pair cell solution.The SF is asymmetric single-pair cell vortex for smaller values of *Tr*, on the other hand, symmetric flow pattern appears for larger value of *Tr* because of weak Coriolis force and creates extra small vortices, visible right side of the duct, due to Dean instability (Centrifugal instability). It is observed that the upper part of the solution curve i.e from point *b* to point *g* is composed of symmetric 2-to 4-pair cell solution though the rotation parameter decreases. Note: The reasons for symmetry of SF are the same as previousely explained in sub-section 4.1.1. The extra vortices, called *Dean vortices*, intensify heat transfer. It is found that the maximum zone of the contours of AF is divided into a small number of high velocity zones in the upper part of the solution curve and the AF is slightly moved to right side of the duct for increasing *Tr*.

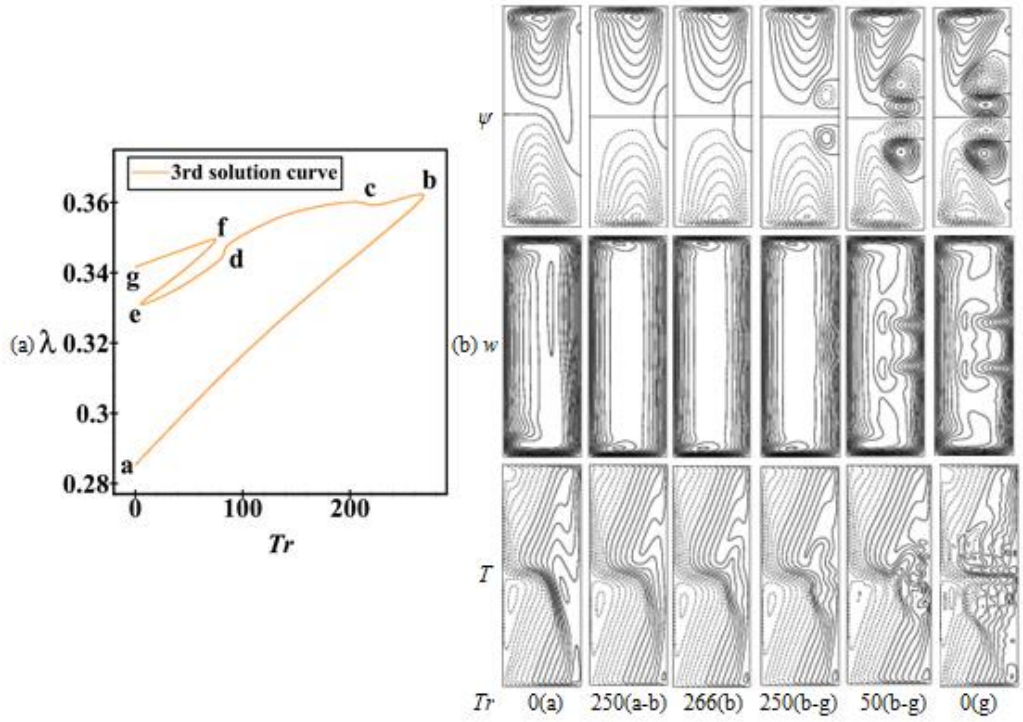

Fig. 6: (a) The 3rd solution curve for $\beta = 0.5$ and $0 \leq Tr \leq 2000$ (b) SF (top), AF (middle) and energy distribution (bottom) for different Tr at $\beta = 0.5$.

4.1.4 The fourth solution curve

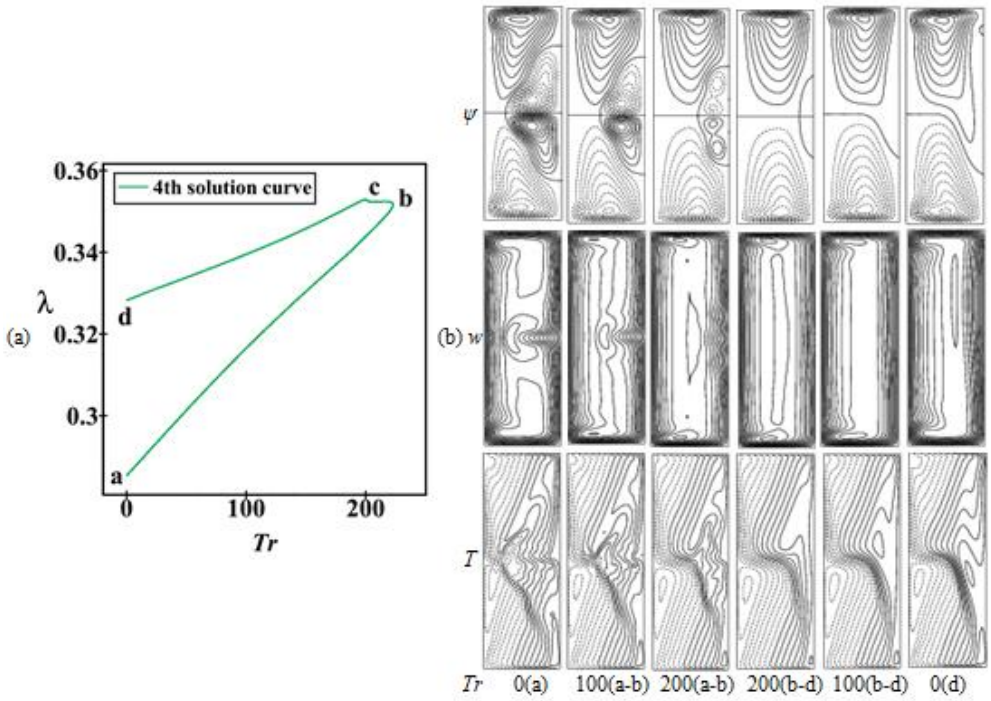

Fig. 7: (a) The 4th solution curve for $\beta = 0.5$ and $0 \leq Tr \leq 2000$ (b) SF (top), AF (middle) and energy distribution (bottom) for different Tr at $\beta = 0.5$.

Figure 7(a) represents the fourth SS curve which is shown by a green-colored solid line. It is a small-ranged branch and has only two smooth turnings. Figure7(b) shows velocity and energy profiles on the fourth solution curve consists of asymmetric single-pair cell and symmetric 2-pair cell solutions.

4.1.5 The fifth solution curve

The 5th steady solution curve is pictured by a pink colored solid line (refer Fig. 8(a)). It is the smallest-ranged branch obtained in this study. It has a single turning at point c ($Tr \approx 118.900858$); (see Fig. 8(a)). Figure 8(b) shows the fifth solution curve consists of asymmetric/symmetric 1- to 3-pair cell. It is observed that the Dean vortices increases near the outside wall on the upper part of the branch as Tr decreases. It is clear from the over all discussion of this section, the energy circulation are homogeneously distributed to the whole section transmitting heat from lower edge to the fluid.

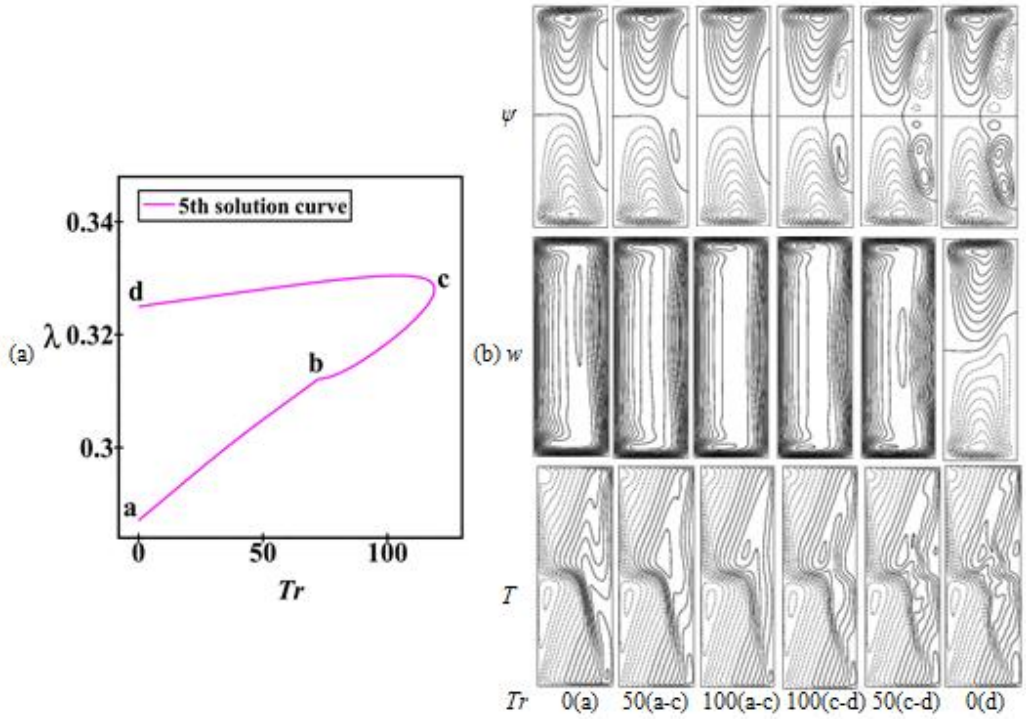

Fig. 8: (a) The 5th solution curve for $\beta = 0.5$ and $0 \leq Tr \leq 2000$ (b) SF (top), AF (middle) and energy distribution (bottom) for different Tr at $\beta = 0.5$.

4.1.6 Vortex generation of the steady solution curves

A schematic representation of the longitudinal vortex-generation of the above-mentioned SFs is observed for various values of Tr for curvature $\beta = 0.5$ as presented in Fig.9. We draw a bar diagram to describe the vortex generation of secondary flows (SF) on various solution curves for $\beta = 0.5$ in the Taylor number vs. number of vortices ($Tr - \theta$) plane. Figure 9 shows vortex generation of SFs on various curves of SS, where it can be seen that 1- to 4-pair cell are produced at the same value of Tr on the above five curves of SSs. Clearly, maximum 4-pair cell is observed at $Tr = 0$; however, as Tr is increased that means the duct rotation is high, the number of secondary vortices decreases and we get only 1-pair vortex solution. It is observed that there are different number of vortices on the same curve for the same value of Tr.

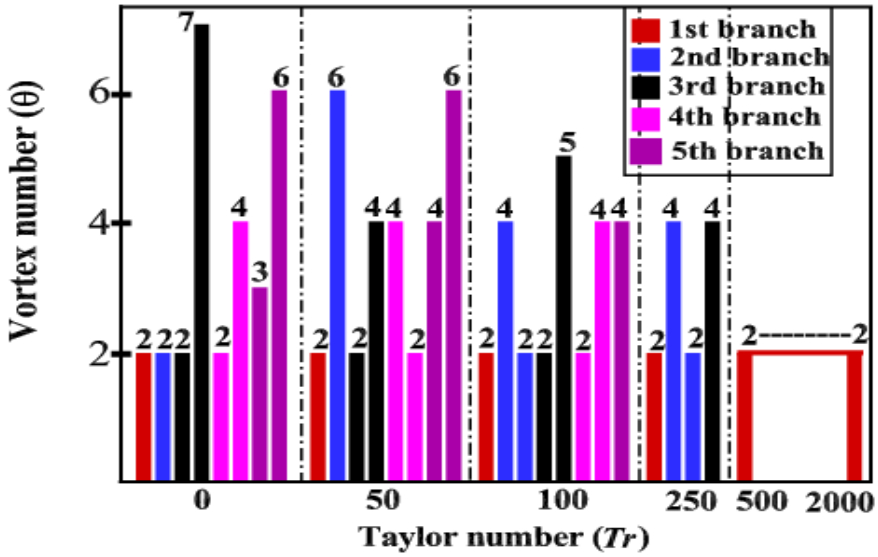

Fig. 9: Vortex generation of secondary flows in the Taylor number versus number of vortices ($Tr - \theta$) plane for $\beta = 0.5$.

4.2 Oscillating behavior and phase spaces

In this subsection, a detailed examination of the flow oscillating behavior and transition into various regimes ranging from 0 to 2000 for $\beta = 0.5$, $Gr = 100$ and $Dn = 1000$ is presented. Here, we tried to figure out the oscillating behavior of λ for $Tr = 0$, $Tr = 100$, $Tr = 262$, $Tr = 268$, $Tr = 290$, $Tr = 295$, $Tr = 2000$ at $\beta = 0.5$. It is found that the oscillating flow is chaotic for $Tr = 0$, $Tr = 100$ and $Tr = 262$ as shown in Figures 10(a), 11(a) and 12(a), respectively. In Figures 10(b), 11(b) and 12(b) we show chaotic flow to be more pronounced, drawing phase space diagram, in the less can be observed in Figures 10(a), 11(a) and 12(a) respectively in the λ - γ plane, where $\gamma = \int\int \psi dxdy$. Figures 10(b), 11(b) and 12(b) conform the chaotic stage for $Tr = 0$, $Tr = 100$ and $Tr = 262$, the flow is a *transitional chaos* (Mondal *et al*., 2007) that turns into another transient flow as Tr increases. The flow oscillates irregularly between axisymmetric 1-pair to 3-pair cell, 2-pair to 3-pair cell and 1-pair to 2-pair cell for $Tr = 0$, $Tr = 100$ and $Tr = 262$ respectively (see Figs. 10(c), 11(c) and 12(c)). The energy circulation are homogeneously distributed to the whole section on the other hand, the streamlines velocity profiles and energy distribution are distributed symmetrically for $Tr = 262$.

When the value of Tr is gradually increased at $Tr = 268$, the transitional chaotic flow transforms into multi-periodic flow with axisymmetric 1-pair to 2-pair cell vortices (Figs. 13(a) and 13(c)). Figure 13(b) shows time-advancement result of the flow which clearly multi-periodic. The alternation of flow state takes place between $Tr = 262$ and $Tr = 268$. With further increase of Tr, the flow transformation occurs at $Tr = 290$ where the multi-periodic flow transforms into periodic with axisymmetric 1-pair vortex solution (Fig. 14(a)). In fact, the noticed transient flow is a traveling-wave solution referred to Yanase *et al*. (2008) for details of travelling-wave. To see the flow state further explicitly, phase-space are exposed for $Tr = 290$ (see Fig. 14(b)), clearly, the flow oscillation is periodic. Streamlines and energy distributions are symmetrically distributed (Fig. 14(c)). As Tr values are further increased, a steady-state solution with single-pair vortex takes place at $Tr = 295$ and it is clear that as Tr increases from 295 to 2000, the flow remains unchanged as seen in Figures 15(a), 16(a), 15(b) and 16(b). It is seen that the conversion from periodic to steady-state elucidation attains between $Tr = 290$ and $Tr = 295$.

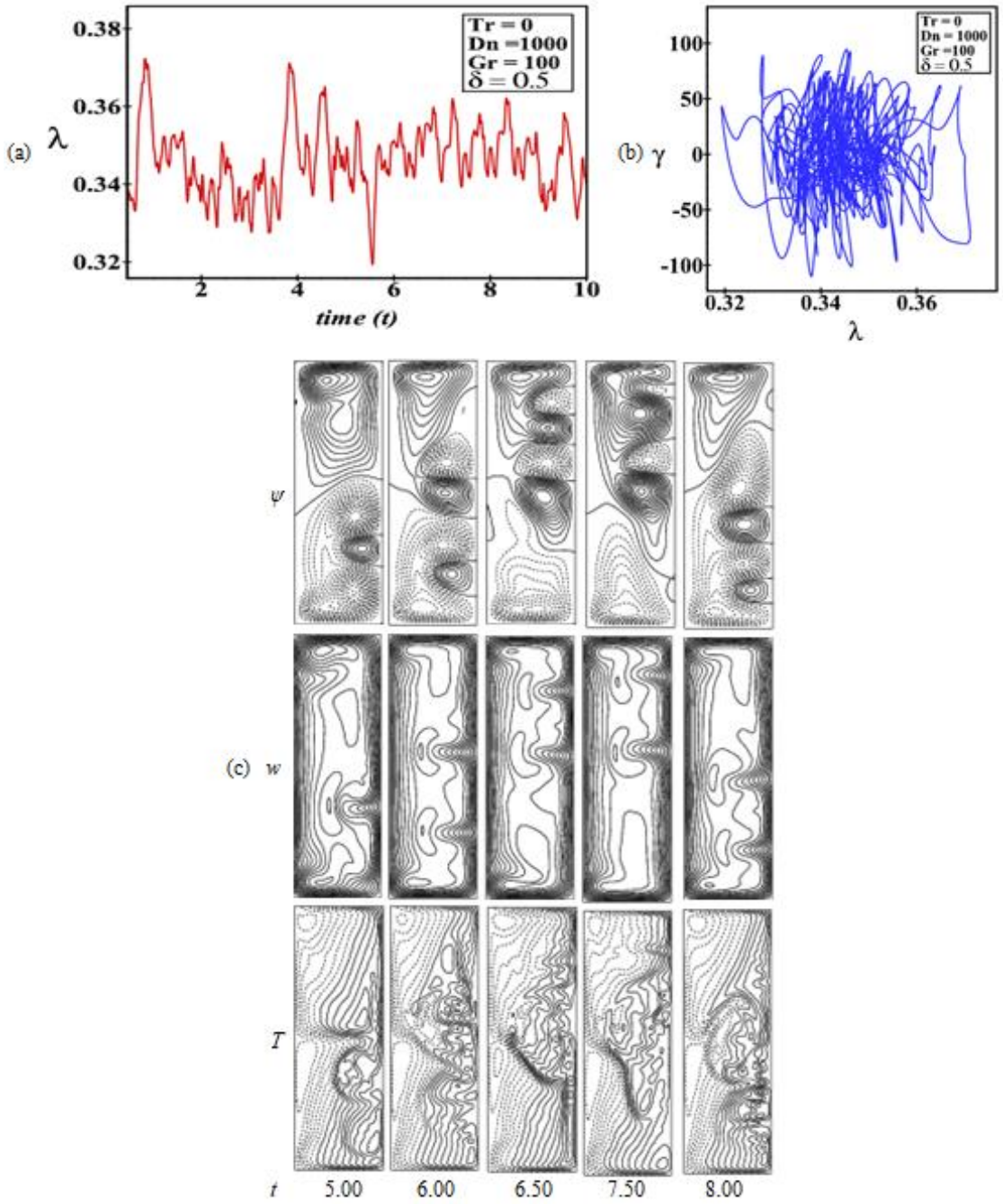

Fig. 10: Time-progress, phase-space and streamlines for $Tr = 0$ (a) Time advancement. (b) Phase-portrait in the $\lambda - \gamma$ plane (c) SF (top), AF (middle) and energy distribution (bottom) for $5.00 \leq t \leq 8.00$.

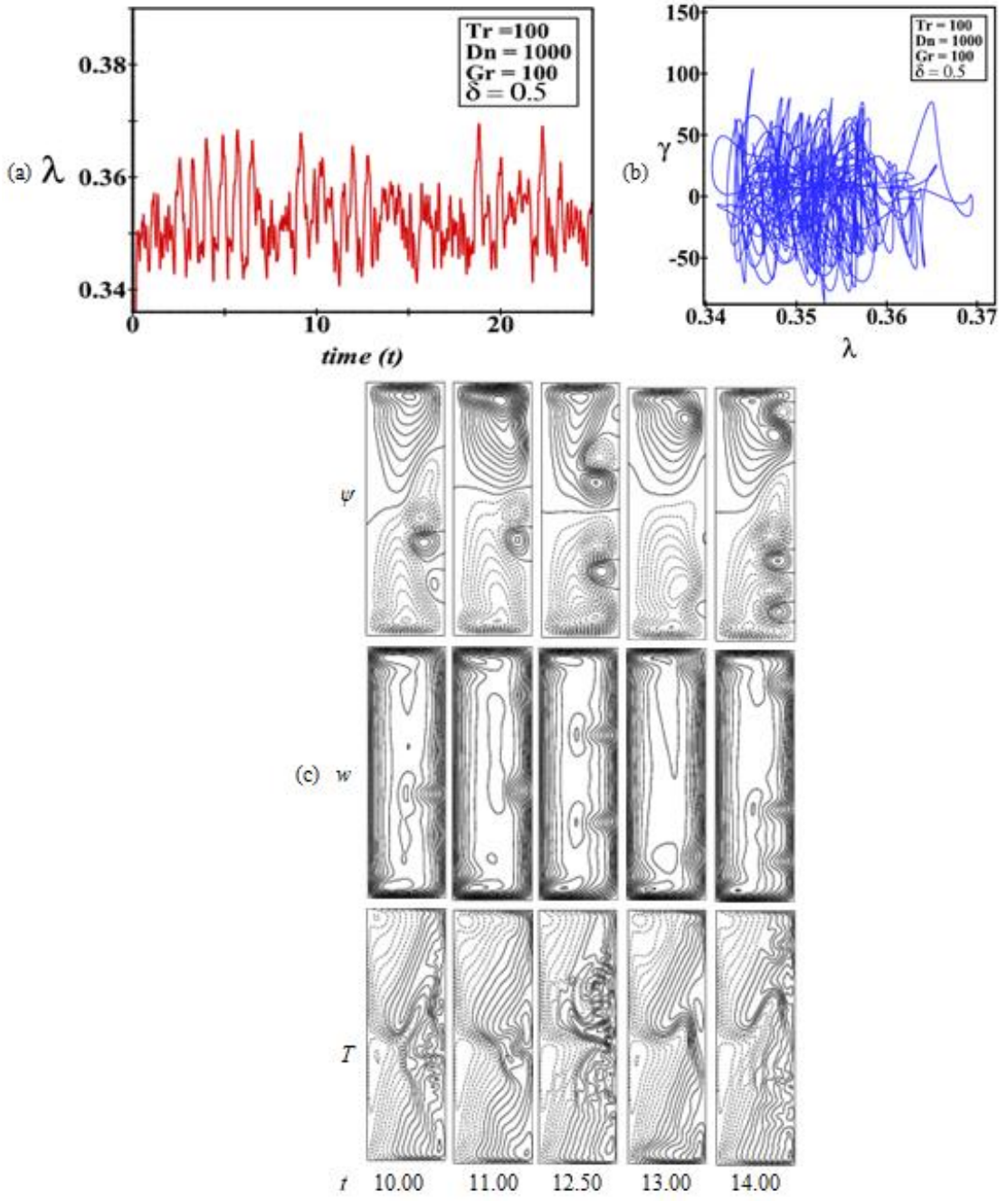

Fig. 11: Time-progress, phase-space and streamlines for Tr = 100 (a) Time advancement. (b) Phase-portrait in the $\lambda - \gamma$ plane (c) SF (top), AF (middle) and energy distribution (bottom) for $10.00 \leq t \leq 14.00$.

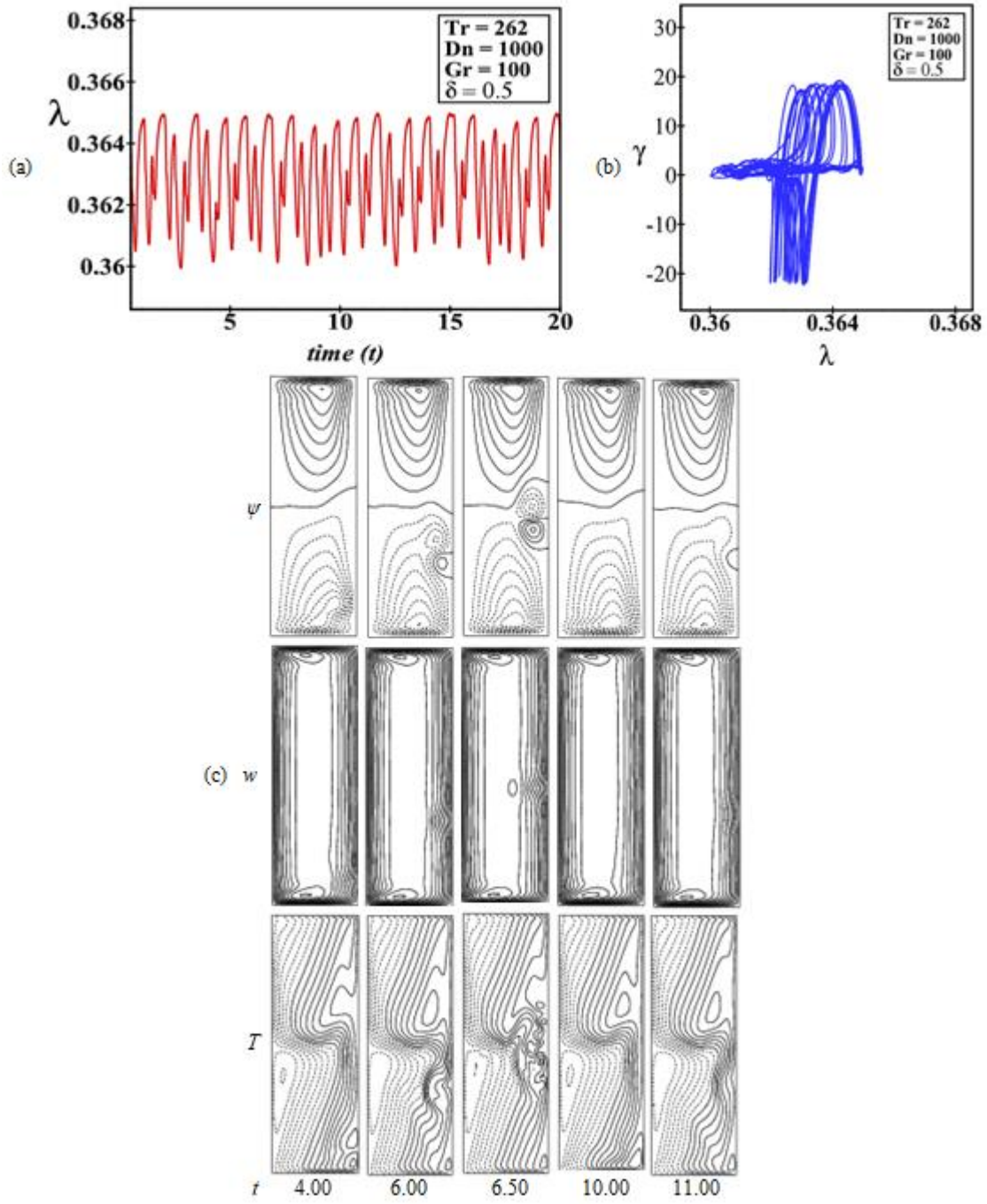

Fig. 12: Time-progress, phase-space and streamlines for Tr = 262 (a) Time advancement. (b) Phase-portrait in the $\lambda - \gamma$ plane (c) SF (top), AF (middle) and energy distribution (bottom) for $4.00 \leq t \leq 11.00$.

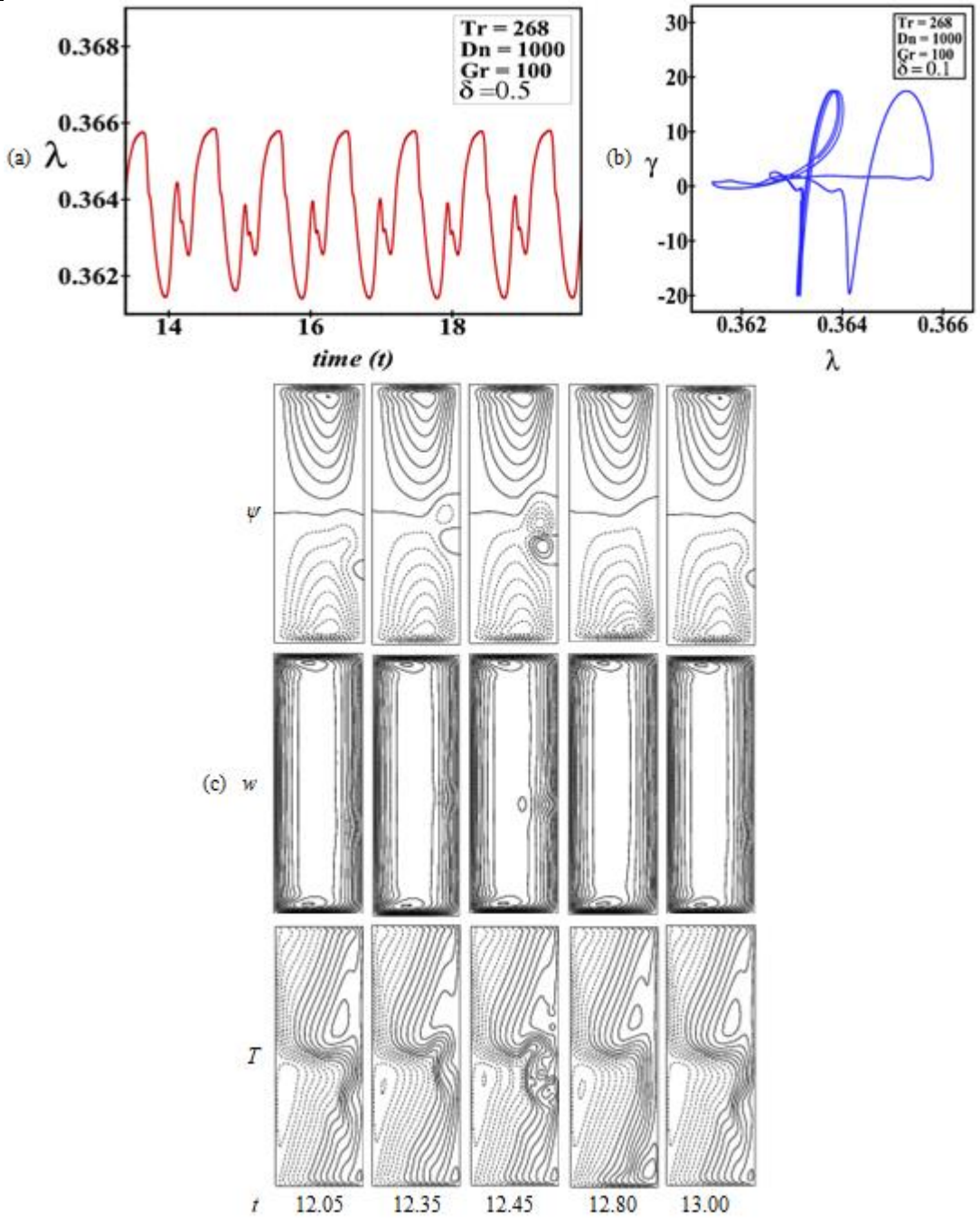

Fig. 13: Time-progress, phase-space and streamlines for Tr = 268 (a) Time advancement. (b) Phase-portrait in the $\lambda - \gamma$ plane (c) SF (top), AF (middle) and energy distribution (bottom) for $12.05 \leq t \leq 13.00$.

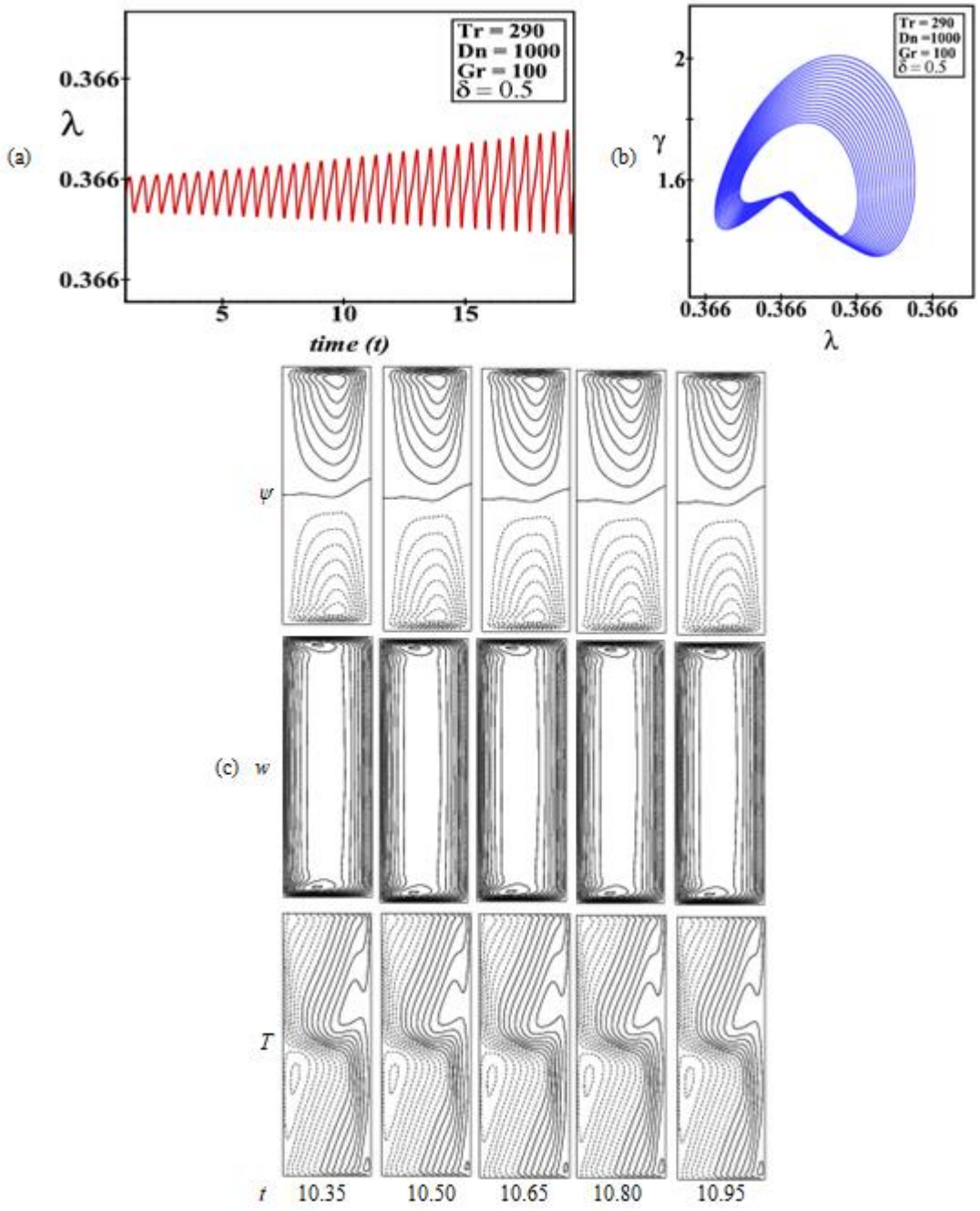

Fig. 14: Time-progress, phase-space and streamlines for Tr = 290 (a) Time advancement. (b) Phase-portrait in the $\lambda - \gamma$ plane (c) SF (top), AF (middle) and energy distribution (bottom) for $10.35 \leq t \leq 10.95$.

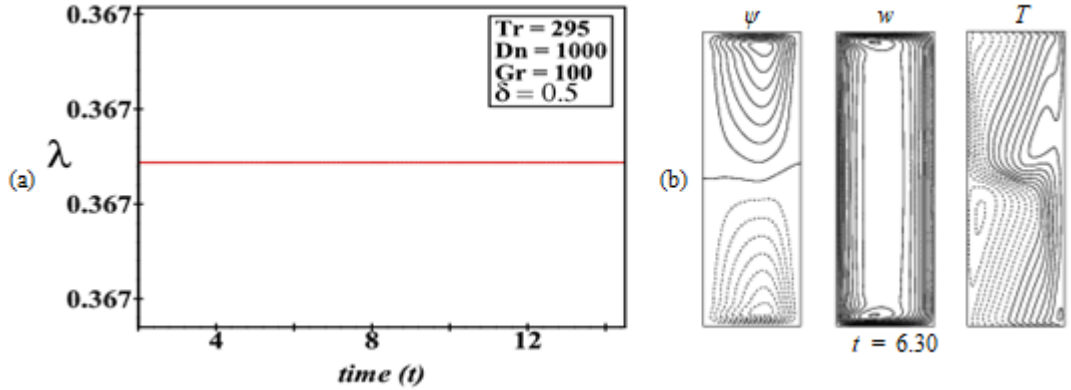

Fig. 15: Time-progress, phase-space and streamlines for *Tr* = 295 (a) Time advancement (b) SF (left), AF (middle) and energy distribution (right) at *t* = 6.30.

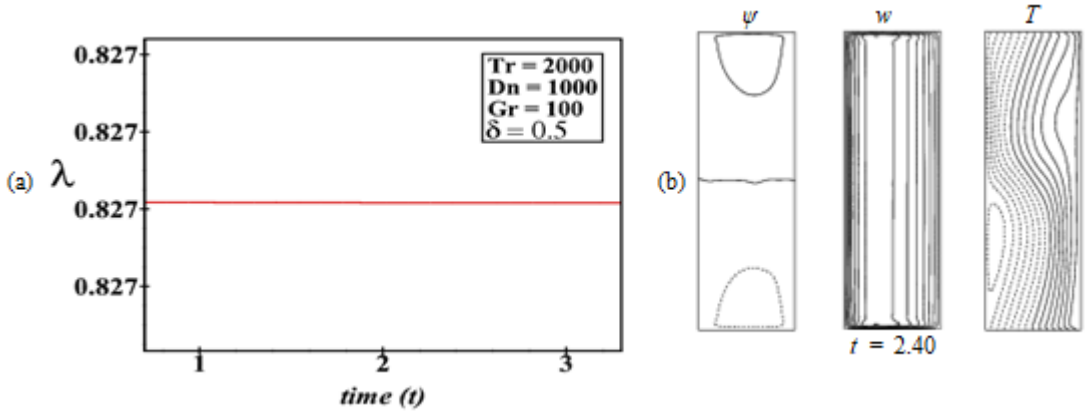

Fig. 16: Time-progress, phase-space and streamlines for *Tr* = 2000 (a) Time advancement (b) SF (left), AF (middle) and energy distribution (right) at *t* = 2.40.

4.3 Vortex generation of the time-dependent solutions

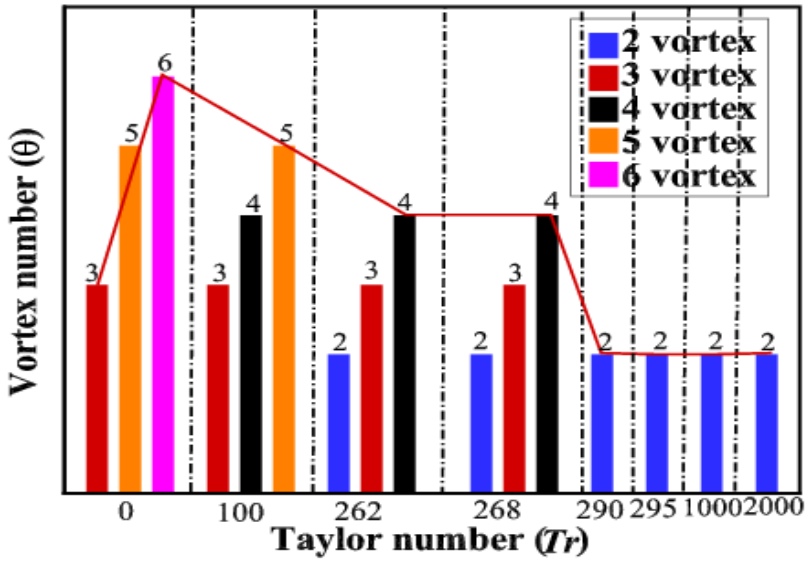

Fig. 17: Vortex generation of secondary flows on time-advancement solutions for β = 0.5.

A schematic representation of the longitudinal vortex-generation of secondary flows corresponding to the time-advancement solutions in the (*Tr* - θ) plane for positive rotation at β = 0.5 is presented in Fig.17. It is found that 2-pair to 3-pair vortices are produced at the same value of *Tr*. Clearly, maximum 3-pairs cell is observed at *Tr* = 0; however, as *Tr* is increased (*Tr* ≥ 290) the flow becomes steady-state and the number of secondary vortices decreases and we get only axisymmetric single-pair (2-vortex) cell solution. The reason is that strong centrifugal force and Coriolis force act in an opposite manner where buoyancy force is predominated and consequently number of secondary vortices decreases.

4.4 Convective heat transfer

In this subsection, we discuss the effect of rotation on CHT between the fluid and the heated wall which is quantitatively evaluated by temperature gradients (TG) at differentially heated walls. In Figures 18(a) and 18(b), the variation of TG; $\frac{\partial T}{\partial x}$ is plotted. Figure 18(a) represents the magnitude of TG on the lower side increases in the middle zone around *y* = 0 through the small amplitude oscillation for the heating wall. In Figure 18(b), at the bottom wall, the magnitude of TG tends to decline not only in the central zone *y* = 0 but at other zones as well.

The curve very fastly approaches to an approximately flat-shape for Tr = 175 and Tr = 200. It is also found that the peak TG appears at the central region for Tr = 50.

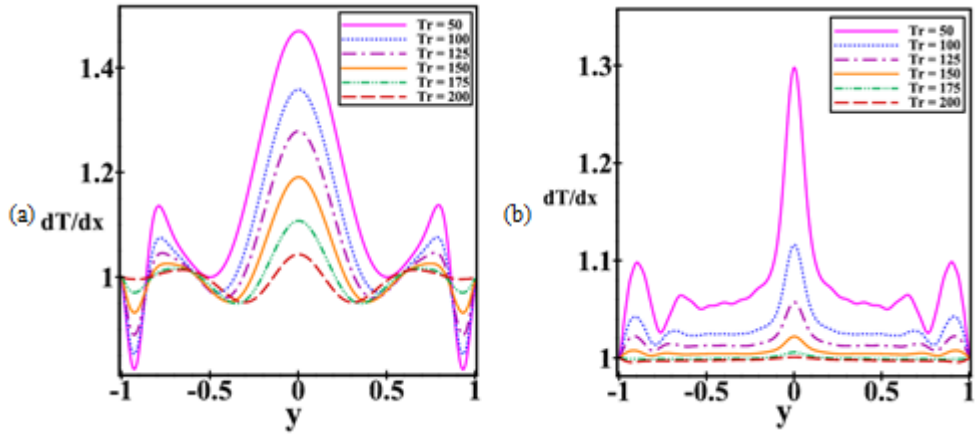

Fig. 18: (a) TG at the cooling wall, (b) TG at the heated wall

4.5 Validation of the numerical result

Here, we present the comparative study of the our numerical and experimental investigations provided for both curved square duct (CSD) and CRD flow. Figure 19 presents a relative comparison of our numerical findings with the laboratory-based experiment by Chandratilleke (2001) for a CRD flow where Ar = 2. Figure 19 shows, a well justification between our present computations and the experimental measurements is exist, which justifies the accuracy of the present numerical study.

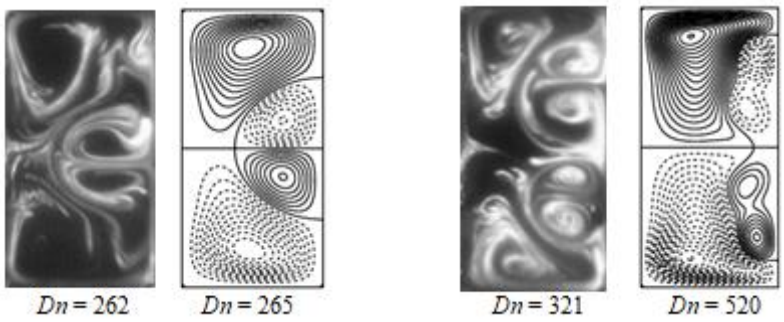

Fig. 19: Experimental vs. computational results. Left: Experimental result by Chandratilleke (2001) for curved rectangular duct flow of aspect ratio 2 and Right: computational result by the authors.

5. Concluding Remarks

The continuing study determines a spectral-based numerical approach on fluid flow, energy distribution and heat transfer through a CRD in at rotating system with the bottom edge heating and the top edge cooling. A wide-range of Taylor numbers (Tr) from 0 to 2000 is considered for constant curvature ratio β = 0.5 and aspect ratio 3. The numerical findings are validated with the available experimental data. The following conclusions have been drawn from the present study;

- An asymmetric five steady solution curves have been found consisting of 2- to 8-cell solution on various branches.
- Time-history as well as phase-plot analysis demonstrates that transient flow develops in the consequence "*chaotic → multi-periodic → periodic → steady-state*" as Tr is increased.
- Velocity contours show that there exist 2-cell flow for the steady case, 2- to 4-cell for the periodic or multi-periodic oscillation while 3- to 6-cell for the chaotic oscillation. Maximum 6-cell solution is observed for the chaotic oscillation at small Tr and the number of secondary vortices gradually decreases as Tr is increased.
- Heat transfer is increased with the increase of rotation and it is enhanced substantially by the chaotic solutions than other flow states.
- A strong interaction between the heating-induced buoyancy force and centrifugal-Coriolis instability is noticed that stimulates fluid mixing and subsequently enhances heat transfer in the fluid.

References

Bara, B. M., Nandakumar, K. and Masliyah, J. H. (1992): An Experimental and Numerical Study of the Dean Problem: Flow Development towards Two-Dimensional Multiple Solutions, Journal of Fluid Mechanics, Vol. 244, No. 1, pp. 339-376. https://doi.org/10.1017/S0022112092003100

Baylis, J. A. (1971): Experiments on Laminar Flow in Curved Channels of Square Section, Journal of Fluid Mechanics, Vol. 48, No. 3, pp. 417–422. https://doi.org/10.1017/S0022112071001678

Berger, S.A., Talbot, L. and Yao, L. S. (1983): Flow in Curved Pipes, Annual Review Fluid Mechanics, Vol. 35, pp. 461-512. https://doi.org/10.1146/annurev.fl.15.010183.002333

Chandratilleke T. T. (2001): Secondary flow characteristics and convective heat transfer in a curved rectangular duct with external heating, 5th World Conference on Experimental Heat Transfer, Fluid Mechanics and Thermodynamics [ExHFT-5], Thessaloniki, Greece.

Chandratilleke, T. T. and Nursubyakto. (2003): Numerical prediction of secondary flow and convective heat transfer in externally heated curved rectangular ducts, International Journal of Thermal Science, Vol. 42, No.2, pp. 187-198. https://doi.org/10.1016/S1290-0729(02)00018-2

Chandratilleke, T. T, Nadim, N. and Narayanaswamy, R. (2012): Vortex structure-based analysis of laminar flow behavior and thermal characteristics in curved ducts, International Journal of Thermal Science, Vol. 59, pp. 75-86. https://doi.org/10.1016/j.ijthermalsci.2012.04.014

Cheng, K.C., Lin, R.C. and Ou, J.W. (1975): Graetz problem in curved square channels, Journal of Heat Transfer, Vol. 97, pp. 244-248. https://doi.org/10.1115/1.3450348

Daskopoulos, P. and Lenhoff A. M. (1989): Flow in Curved Ducts: Bifurcation Structure for Stationary Ducts, Journal of Fluid Mechanics, Vol. 203, pp. 125-148. https://doi.org/10.1017/S0022112089001400

Dean, W. R. (1927): Note on the motion of a fluid in a curved pipe, Philos. Mag., Vol. 20, pp. 208–233. https://doi.org/10.1112/S0025579300001947

Dean, W. R. (1928): The streamline motion of a fluid in a curved pipe, Philos. Mag., Vol. 30, pp. 673–693. https://doi.org/10.1080/14786440408564513

Hasan, M. S., Mondal, R.N. and Lorenzini, G. (2021): Centrifugal-Coriolis instability through a rotating curved square duct with bottom wall heating and cooling from the ceiling, AIP Conference Proceedings, Vol. 2324, No. 040007. https://doi.org/10.1063/5.0037784

Humphrey, J. A. C., Taylor, A. M. K. and Whitelaw, J. H. (1977): Laminar Flow in a Square Duct of Strong Curvature, Journal of Fluid Mechanics, Vol. 83, No. 3, pp. 509–527. https://doi.org/10.1017/S0022112077001311

Ito, H. (1987): Flow in Curved Pipes, JSME International Journal, Vol. 30, pp. 543-552. https://doi.org/10.1299/jsme1987.30.543

Ligrani, P. M. and Niver, R. D. (1988): Flow Visualization of Dean Vortices in a Curved Channel with 40 to 1 Aspect Ratio, Physics of Fluids, Vol. 31, No. 12, pp. 3605-3617. https://doi.org/10.1063/1.866877

Li, Y., Wang, X., Yuan, S. and Tan, S. K. (2016): Flow development in curved rectangular ducts with continuously varying curvature, Experimental Thermal and Fluid Science, Vol. 75, pp. 1-15. https://doi.org/10.1016/j.expthermflusci.2016.01.012

Ludwieg, H. (1951); Die Ausgebildete kanalstromung in einemrotierenden System, Journal of Applied Mathematics and Mechanics, Vo. 31, pp. 291-296.

Miyazaki, H. (1971): Combined free and force convective heat transfer and fluid flow in a rotating curved circular tube, International Journal of Heat Mass Transfer, Vol. 14, pp. 1295-1309. https://doi.org/10.1016/0017-9310(71)90179-7

Miyazaki, H. (1973): Combined free and force convective heat transfer and fluid flow in rotating curved rectangular tubes, Trans. ASMEC: Heat Transfer, Vol. 95, pp. 64-71. https://doi.org/10.1115/1.3450006

Mondal, R. N. (2006): Isothermal and Non-isothermal Flows Through Curved ducts with Square and Rectangular Cross Sections, Ph.D. Thesis, Department of Mechanical and Systems Engineering, Okayama University, Japan.

Mondal, R. N., Kaga Y., Hyakutake T. and Yanase S. (2006): Effects of Curvature and Convective Heat Transfer in Curved Square Duct Flows, ASME Trans. Journal of Fluids Engineering, Vol. 128, No. 9, pp. 1013-1023. https://doi.org/10.1115/1.2236131

Mondal, R.N., Kaga, Y., Hyakutake, T. and Yanase, S. (2007): Bifurcation diagram for two-dimensional steady flow and unsteady solutions in a curved square duct, Fluid Dynamics Research, Vol. 39, pp. 413-446. https://doi.org/10.1016/j.fluiddyn.2006.10.001

Mondal, R. N., Alam, M. M. and Yanase S. (2007): Numerical Prediction of Non-Isothermal Flows through a Rotating Curved Duct with Square Cross Section, Thammasat International Journal of Science and Technology, Vol. 12, pp. 24-43. https://ph02.tci-thaijo.org/index.php/SciTechAsia/article/view/41507
Mondal, R. N., Ray, S. C. and Yanase S. (2015): Combined effects of centrifugal and Coriolis instability of the flow through a rotating curved duct with rectangular cross section, Open Journal of Fluid Dynamics, Vol. 4, No. 4, pp. 1-14. https://doi.org/10.4236/ojfd.2014.41001
Mondal, R. N, Watanabe, T., Hossain, M. A. and Yanase, S. (2017): Vortex-Structure and Unsteady Solutions with Convective Heat Transfer trough a Curved Duct, Journal of Thermophysics and Heat Transfer, Vol. 31, No. 1, pp. 243-254. https://doi.org/10.2514/1.T4913
Mondal, R. N., Hasan, M. S., Islam, M. S., Islam, M. Z. and Saha S. C. (2021): A Computational Study on Fluid Flow and Heat Transfer Through a Rotating Curved Duct with Rectangular Cross Section, International Journal of Heat and Technology, Vol. 39, No. 4, pp. 1213-1224. https://doi.org/10.18280/ijht.390419
Nandakumar, K. and Masliyah, J. H. (1986): Swirling Flow and Heat Transfer in Coiled and Twisted Pipes, Adv. Transport Process., Vol. 4, pp. 49-112.
Nowruzi, H., Ghassemi, H. and Nourazar, S. S. (2019): Linear Hydrodynamic Stability of Fluid Flow in Curved Rectangular Ducts: Semi-Analytical Study, Journal of Mechanics, Vol. 35, No. 5, pp. 747-765. https://doi.org/10.1017/jmech.2019.5
Ray, S. C., Hasan, M. S., Mondal, R. N. (2020): On the Onset of Hydrodynamic Instability with Convective Heat Transfer Through a Rotating Curved Rectangular Duct, Mathematical Modelling of Engineering Problems, Vol. 7, No. 1, pp. 31-44. https://doi.org/10.18280/mmep.070105
Selmi, M., Namadakumar, K., and Finlay, W.H. (1994): A bifurcation study of viscous flow through a rotating curved duct, Journal of Fluid Mechanics, Vol. 262, pp. 353-375. https://doi.org/10.1017/S0022112094000534
Selmi, M., Namadakumar, K. and Finlay, W.H. (1999): Bifurcation study of flow through rotating curved ducts, Physics of Fluids, Vo. 11, No. 8, pp. 2030-2043. https://doi.org/10.1063/1.870066
Shantini, W. and Nandakumar, K. (1986): Bifurcation phenomena of generalized Newtonian fluids in curved rectangular ducts, Journal of Non-Newtonian Fluid Mechanics, Vol. 22, pp. 35-60. https://doi.org/10.1016/0377-0257(86)80003-9
Sugiyama S., Hayashi T. and Yamazaki K. (1983): Flow characteristics in the curved rectangular channels (Visualization of secondary flow), Bulletin of the JSME, Vol. 26, No. 216, pp. 964-969. https://doi.org/10.1299/jsme1958.26.964
Wang, L. Q. and Yang, T. L. (2004): Multiplicity and Stability of Convection in Curved Ducts: Review and Progress, Advances in Heat Transfer, Vol. 38, pp. 203-256. https://doi.org/10.1016/S0065-2717(04)38004-4
Wang, L. and Yang, T. (2005), Periodic Oscillation in Curved Duct Flows, Physica D, Vol. 200, pp. 296-302. https://doi.org/10.1016/j.physd.2004.11.003
Watanabe, T. and Yanase, S. (2013): Bifurcation Study of Three-Dimensional Solutions of the Curved Square-Duct Flow, Journal of the Physical Society of Japan, Vol. 82, No. 0744321-9. https://doi.org/10.7566/JPSJ.82.074402
Yamamoto K., Xiaoyun W., Kazuo N. and Yasutaka H. (2006): Visualization of Taylor-Dean flow in a curved duct of square cross section, Fluid Dynamics Research, Vol. 38, pp. 1-18. https://doi.org/10.1016/j.fluiddyn.2005.09.002
Yanase, S. and Nishiyama, K. (1988): On the Bifurcation of Laminar Flows through a Curved Rectangular Tube, Journal of the Physical Society of Japan, Vol. 57, pp. 3790-3795. https://doi.org/10.1143/JPSJ.57.3790
Yanase S., Kaga Y. and Daikai R. (2002): Laminar flow through a curved rectangular duct over a wide range of aspect ratio, Fluid Dynamics Research, Vol. 31, pp. 151-83. https://doi.org/10.1016/S0169-5983(02)00103-X
Yanase, S., Mondal, R N. and Kaga, Y. (2005): Numerical Study of Non-Isothermal Flow with Convective Heat Transfer in a Curved Rectangular Duct, International Journal of Thermal Sciences, Vol. 44, pp. 1047-1060. https://doi.org/10.1016/j.ijthermalsci.2005.03.013
Yanase, S., Watanabe, T. and Hyakutake, T. (2008): Traveling-wave solutions of the flow in a curved-square duct, Physics of fluids, Vol. 20, No. 124101. https://doi.org/10.1063/1.3029703
Zhang, W., Wei, Y., Dou, H.S. and Zhu, Z. (2018): Transient behaviors of mixed convection in a square enclosure with an inner impulsively rotating circular cylinder, International Communications in Heat and Mass Transfer, Vol. 98, pp. 143-154. https://doi.org/10.1016/j.icheatmasstransfer.2018.08.016